Gene polymorphism linked to increased asthma and IBD risk alters gasdermin-B structure, a sulfatide and phosphoinositide binding protein

Kinlin L. Chao[a], Liudmila Kulakova[a], and Osnat Herzberg[a,b,1]

[a]Institute for Bioscience and Biotechnology Research, University of Maryland, Rockville, MD 20850; and [b]Department of Chemistry and Biochemistry, University of Maryland, College Park, MD 20742

Edited by Ada Yonath, Weizmann Institute of Science, Rehovot, Israel, and approved December 23, 2016 (received for review October 9, 2016)

The exact function of human gasdermin-B (GSDMB), which regulates differentiation and growth of epithelial cells, is yet to be elucidated. In human epidermal growth factor receptor 2 (HER2)-positive breast cancer, *GSDMB* gene amplification and protein overexpression indicate a poor response to HER2-targeted therapy. Genome-wide association studies revealed a correlation between *GSDMB* SNPs and an increased susceptibility to Crohn's disease, ulcerative colitis, and asthma. The N- and C-terminal domains of all gasdermins possess lipid-binding and regulatory activities, respectively. Inflammatory caspases cleave gasdermin-D in the interdomain linker but not GSDMB. The cleaved N-terminal domain binds phosphoinositides and cardiolipin, forms membrane-disrupting pores, and executes pyroptosis. We show that both full-length GSDMB and the N-terminal domain bind to nitrocellulose membranes immobilized with phosphoinositides or sulfatide, but not with cardiolipin. In addition, the GSDMB N-terminal domain binds liposomes containing sulfatide. The crystal structure of the GSDMB C-terminal domain reveals the structural impact of the amino acids encoded by SNPs that are linked to asthma and inflammatory bowel disease (IBD). A loop that carries the polymorphism amino acids corresponding to healthy individuals (Gly299:Pro306) exhibits high conformational flexibility, whereas the loop carrying amino acids found in individuals with increased disease risk (Arg299:Ser306) exhibits a well-defined conformation and higher positive surface charge. Apoptotic executioner caspase-3, -6, and -7, but not the inflammatory caspases, cleave GSDMB at $_{88}$DNVD$_{91}$ within the N-terminal domain. Selective sulfatide binding may indicate possible function for GSDMB in the cellular sulfatide transport.

GSDMB | X-ray crystallography | disease risk polymorphism | complex trait inflammatory disease | lipid binding

The human genome encodes four gasdermin (GSDM) proteins (GSDMA to -D) that are expressed in epithelial cells and have regulatory functions in normal cell proliferation and differentiation and the maintenance of the epithelial cell barrier (1, 2). The mouse genome contains three clusters of *GSDM* genes, encoding eight GSDMs (Gsdma1 to -3, Gsdmc1 to -4, and Gsdmd), but lacks the analog of the human GSDMB (also known as GSDML or PRO2521) (1). Based on the differential protein expressions in gastric and esophageal cancers, human GSDMA, GSDMC, and GSDMD are considered tumor suppressors whereas an overexpression of GSDMB in gastric, uterine cervix, and breast cancers was accompanied by tumor progression and metastasis (3–8). The overexpression of GSDMC in metastatic melanoma cells is an exception to its apoptotic role (9). In addition to cancer, genome-wide association studies (GWAS) have revealed a correlation between single nucleotide polymorphisms (SNPs) in both the protein coding and transcriptional regulatory regions of the neighboring genes *GSDMA*, *GSDMB*, and *ORDML3* in the 17q12.2.1 loci and susceptibility to diseases such as asthma (10–20), type 1 diabetes (21, 22), Crohn's disease, ulcerative colitis (22, 23), and rheumatoid arteritis (22, 24). The mechanisms by which these SNPs affect susceptibility to developing complex-trait inflammatory diseases are unknown.

The recent crystal structure of mouse Gsdma3 [an ortholog of GSDMA; Protein Data Bank (PDB) ID code 5B5R] revealed a two-domain protein connected by a long flexible linker. The N-terminal domain folds into an α+β structure, and the C-terminal domain comprises predominantly α-helices (25). Multiple amino acid sequence alignment of GSDM family members, ∼400 to 500 aa in length, reveals 9% sequence identity among the four human GSDM paralogues (Fig. 1). However, pairwise alignments show 29%, 24%, and 25% amino acid sequence identity between GSDMB and its paralogues, GSDMA, GSDMC, and GSDMD, respectively, suggesting that all GSDMs adopt the same overall fold as that of Gsdma3.

Recent reports identified the N-terminal domain of mouse Gsdma3, expressed in HEK293 and HaCatT cells, as well as Gsdma3 mutants that cause skin and hair defects in mice, to promote cell death (26, 27). Similarly, the N-terminal domains of human GSDMA, GSDMC, and GSDMD caused autophagy whereas the cells remain viable in the presence of the respective C-terminal domains (27). For Gsdam3, the autophagy is initiated when the N-terminal domain binds to heat shock protein 90 (HSP90), and the complex is delivered to the mitochondria by the HSP90/HSP70/Hop complex via the Tom70 importer (26). Subsequent association of the Gsdma3 N-terminal domain with the mitochondrial chaperone TRAP1 promotes the production of reactive oxygen species (ROS), causing mitochondrial stress and loss of membrane integrity. Interestingly, coimmunoprecipitation experiments identified the binding of GSDMB to HSP90β in breast cancer cells (8). The N-terminal domain of GSDMB did not induce autophagy (27),

Significance

The exact function of gasdermin-B, a protein involved in epithelial cell development, is unknown. We provide insights into gasdermin-B function and how it may contribute to cancer progression and genetic susceptibility to asthma and inflammatory bowel disease (IBD). In contrast to other gasdermins, which bind phosphoinositides and cardiolipin only upon cleavage between their N- and C-terminal domains, intact gasdermin-B binds phosphoinositides and, uniquely, sulfatide, a component of the apical membrane of epithelial cells. Polymorphism residues in the C-terminal domain, associated with asthma and IBD, induce structural changes that may affect protein activity. Components of the apical plasma membrane maintain the cell barrier integrity; thus, aberrant sulfatide levels due to changes in the cellular gasdermin-B concentration or activity could affect disease risk.

Author contributions: O.H. conceived the project; K.L.C. and O.H. designed research; K.L.C., L.K., and O.H. performed research; K.L.C. and O.H. analyzed data; and K.L.C. and O.H. wrote the paper.

The authors declare no conflict of interest.

This article is a PNAS Direct Submission.

Data deposition: The atomic coordinates and structure factors have been deposited in the Protein Data Bank, www.pdb.org (PDB ID codes 5TIB, 5TJ2, and 5TJ4).

[1]To whom correspondence should be addressed. Email: osnat@umd.edu.

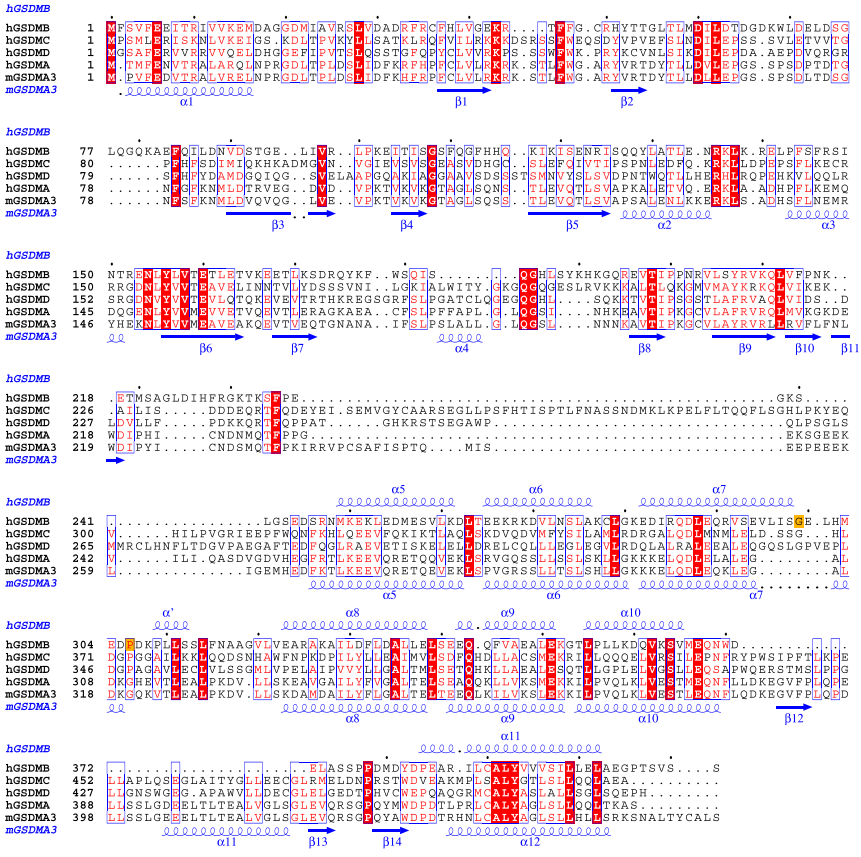

Fig. 1. Structure-based sequence alignment of four human gasdermins (GSDMA to -D) and mouse Gsdma3. Secondary structure elements of the GSDMB C-terminal domain determined in the current study are shown above the GSDMB sequence, and those of Gsdma3 are shown below the Gsdma3 sequence (25). The GSDMB α-helices that form the helix bundle are labeled sequentially, beginning with α5, consistent with the α-helix numbering scheme assigned in the structure of Gsdma3. However, the Gsdma3 α11 is missing in GSDMB; thus, the α11 of GSDMB corresponds to Gsdma3 α12. The short α-helix within the GSDMB polymorphism loop is labeled α′. Invariant residues are highlighted by a red background. Conservatively replaced amino acids are blocked. The two GSDMB polymorphism residues, 299 and 306, are highlighted by an orange background. The alignment was performed using the program T-Coffee (55), and the figure was prepared with ESPript 3 (espript.ibcp.fr/ESPript/ESPript/).

consistent with the cell proliferation activity observed for GSDMB (7). Contrarily, Ding et al. showed that the N-terminal domain of GSDMB does induce pyroptosis of HEK293T cells (25).

For human GSDMD and mouse Gsdmd, the activation of human caspase-1 and mouse caspase-11 (ortholog of human caspase 4/5) by the lipopolysaccharide (LPS) of Gram-negative bacterial pathogens leads to protein cleavage at a specific site (GSDMD $_{272}$FLTD$_{275}$ or Gsdmd $_{274}$LLSD$_{277}$) within their interdomain linker regions (28, 29). In contrast, GSDMA, GSDMB, and GSDMC lack this GSDMD cleavage sequence and are not substrates of caspase-11 (29). Ding et al. showed that the expression of the N-terminal domain of all GSDMs induces pyroptosis of HEK293T cells (25). The N-terminal domains of Gsdma3, GSDMA and GSDMD, but not their full-length proteins, bind phosphoinositides and cardiolipin to disrupt mammalian cell membrane and lyse phosphoinositide- or cardiolipin-containing liposomes by forming pores. Approximately 14 to 16 molecules of the human GSDMD N-terminal domain form ring-like pores in sphingomyelin- or cardiolipin-containing liposomes (30). A recent site-directed mutagenesis study showed that 5 aa ($_2$PSAFE$_6$) in the N-terminal helix of GSDMD are absolutely required for oligomerization and pore formation (31). Concomitant replacements of four positively charged, invariant residues in the N-terminal domain of gasdermin-D proteins (Arg138/Lys146/Arg152/Arg154 in mouse Gsdmd) into Ala/Ser abolished phospholipid and membrane binding and pore forming activity (32). Single residue mutation of the above basic residues did not impair these activities. The mode of phospholipid binding to GSDMD may be unique because only the first arginine residue (Arg138 in Gsdmd) is conserved among all other human and mouse GSDMs.

We undertook structural studies of GSDMB to gain insights into the structural consequences of SNPs, which are linked to increased risk of developing complex-trait inflammatory diseases. Currently, the subcellular location of GSDMB is not well-defined because it was localized primarily in the nucleolus of human epithelial breast (MCF7) and cervical cancer (HeLa) cells (7), or exclusively in the cytoplasm of MCF7 breast cancer cells (8). Human GSDMB has six splice isoforms (Q8TAX9; UniProt Knowledge Base). Isoforms 1 to 4 and isoform 6 differ in the length and sequence of the linker between the N- and C-terminal domains whereas isoform 5 comprises only the C-terminal domain. This study examined the "canonical" GSDMB isoform 1 [411 residues, Q8TAX9-1, identified in National Center for Biotechnology Information (NCBI) as GSDML and GSDMB isoform X3]. Analyses of GWAS data by Pal and Moult identified two *GSDMB* SNPs (dbSNP:rs2305479 and dbSNP:rs2305480) in linkage disequilibrium with a marker of disease risk (22). Based on the numbering scheme of the canonical GSDMB (Uniprot Q8TAX9-1), the rs230549 polymorphism corresponds to a Gly-to-Arg change at position 299, and the rs2305480 polymorphism corresponds to a Pro-to-Ser change at position 306 in the C-terminal domain of GSDMB (GSDMB_C). Further analyses of data compiled by the 1000 Genomes Project Consortium (33) showed that both versions of each SNP (Gly299:Pro306 or Arg299:Ser306) is common in the population and that the two SNPs cooccur in ∼95% of the genomes (22). We have determined three crystal structures of the GSDMB_C domain containing the Arg299:Ser306 sequence encoded by the allele linked to increased risk of complex-trait inflammatory diseases, the Gly299:Pro306 sequence encoded by the alternative allele, and the Gly299:Ser306 sequence that corresponds to one residue from each allele. In addition, we identified the GSDMB's phospholipid binding activities and caspase cleavage profile, which provide additional insights into the function of this protein.

Results and Discussion

Protein Production, Crystallization, and Structure Determination. Initially, GSDMB_C (Glu244–Ser411) was produced as a C-terminal His-tagged protein. The circular dichroism (CD) spectrum of this

protein showed a molecule containing predominantly α-helices, consistent with the secondary structure prediction. The ^{1}H-^{15}N heteronuclear single quantum coherence (HSQC) NMR spectrum of GSDMB_C revealed well-dispersed peaks accounting for most of the amino acids. Nevertheless, this GSDMB_C failed to crystallize. Therefore, we produced the GSDMB_C linked to maltose-binding protein (MBP) using the pMALX vectors (34). These recombinant proteins contain the interdomain linker region (Met220–Lys240) that was systematically truncated by 4- to 5-aa segments. Several recombinant proteins were purified to homogeneity, but only the longest variant (MBP followed by GSDMB Met220–Ser411, MBP-GSDMB_C) yielded crystals. To test the structural impact of disease-associated polymorphisms, four possible variants were crystallized: the two variants found in the population (Gly299:P306 and Arg299:S306) and two alternative combinations that are not observed in the population (Arg299:P306 and Gly299:Ser306). However, the crystals of the MBP-GSDMB_C Arg299:Pro306 variant diffracted X-rays poorly (~7 Å) for analysis. Intriguingly, each variant crystallized in a different space group, with a different number of molecules in the asymmetric unit (Table 1). Together, there are 16 copies of GSDMB_C molecules, each exposed to a different crystal environment. The availability of multiple GSDMB_C molecules increases confidence in the structural analyses.

Overall Structure of the MBP-GSDMB Fusion Protein. In each crystal structure, the MBP-GSDMB_C molecules pack in pairs using both crystallographic and noncrystallographic twofold symmetry axes. Fig. 2*A* presents such a pair in the asymmetric unit of the MBP-GSDMB_C Arg299:Ser306 structure (PDB ID code 5TIB), which form an interface area of 1,250 Å^2, calculated using PISA (35). The corresponding five pairs of the Gly299:Pro306 variant (PDB ID code 5TJ2) and two pairs of the Gly299:Ser306 variant (PDB ID code 5TJ4) molecules form averaged interface areas of 1,588 Å^2 and 1,164 Å^2, respectively. There is no interaction between the two GSDMB_C domains, consistent with the monomeric GSDMB_C eluted from the Superdex 200 size exclusion column. Likewise, the full-length His_6-GSDMB (Gly299:Pro306 variant) also eluted predominantly as monomers. All 16 GSDMB_C domains in the three crystal structures exhibited the same overall fold. The root-mean-square deviations (rmsds) of C^{α} positions of the 10, 4, and 2 molecules in the asymmetric units of the MBP-GSDMB_C Gly299:Pro306, Gly299:Ser306 and Arg299:Ser306 variants were 0.4 to 0.6 Å.

Ensuing the MBP's C-terminal α-helix, a three-alanine linker engineered in the pMALX vector elongates this α-helix (34). The following five GSDMB_C linker residues (Met220–Asp224) further extend the MBP α-helix (Fig. 2), apparently influenced by the presence of MBP. Thus, these five residues may not necessarily form an α-helix in the context of full-length GSDMB. The remaining GSDMB interdomain linker (Ile225–Arg247) adopts a flexible conformation with segments that lack associated electron density, as depicted by a blue dotted line in Fig. 2*B*. Inspection of all 16 molecules in the three crystal structures shows that the extent

Table 1. Data collection and refinement statistics

GSDMB_C variant	Gly299:Pro306	Arg299:Ser306	Gly299:Ser306
Data collection			
Space group	P 2_1	P 4_3 2_1 2	C 2 2 2_1
Cell dimension, Å	a = 89.6, b = 274.6, c = 174.0, β = 96.1	a = 104.1, b = 104.1, c = 252.2	a = 144.0, b = 152.8, c = 255.8
Wavelength, Å	1.0332	0.9793	1.0332
No. of molecules in the ASU	10	2	4
Completeness, %*	92.2 (94.0)	99.8 (100)	99.6 (99.3)
Multiplicity	2.6	5.5	6.1
R_{merge}*,†	0.094 (0.50)	0.112 (0.60)	0.155 (1.052)
$\langle I/\sigma(I)\rangle$*	8.5 (2.2)	10.6 (2.9)	11.3 (2.2)
Refinement statistics			
Resolution range, Å	173–3.5	96.2–2.6	128–2.8
Total no. of reflections	99,563	41,354	65,695
R_{factor}‡/R_{free}§	0.213/0.249	0.184/0.233	0.213/0.252
No. of protein residues	5,462	1,063	2,127
No. of waters	0	286	37
No. of maltose	10	2	4
No. of bicarbonate, Na^+	0, 2	1,1	0, 0
rmsd from ideal geometry			
Bond length, Å	0.016	0.016	0.011
Bond angles, °	1.53	1.49	1.47
Average B factor, Å^2	94.2	47.5	67.0
Protein	94.3	48.0	67.2
Waters	n/a	36.3	32.9
Maltose/ions	64.3	38.1	57.3
Ramachandran plot, %			
Most favored	95.0	98.6	97.3
Allowed	3.7	1.4	2.7
Outliers	1.3	0.0	0.0
Molprobity geometry score (percentile)	2.05 (100)	1.41 (100)	1.33 (100)

ASU, asymmetric unit.

*The values in parentheses are for the highest resolution shell.

†$R_{merge} = \sum_{hkl}[(\sum_j |I_j - \langle I\rangle|)/\sum_j |I_j|]$.

‡$R_{factor} = \sum_{hkl}||F_o| - |F_c||/\sum_{hkl}|F_o|$, where F_o and F_c are the observed and calculated structure factors, respectively.

§R_{free} is computed from 5% of randomly selected reflections and omitted from the refinement.

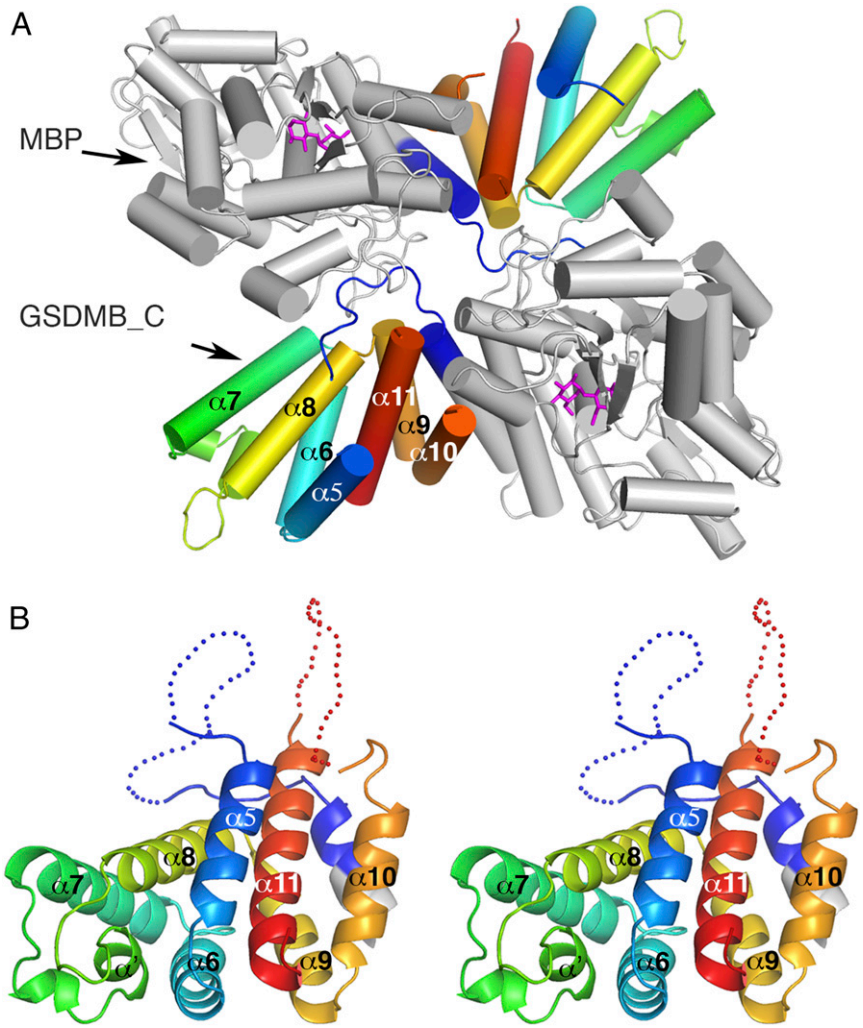

Fig. 2. Structure of human MBP-GSDMB_C. (*A*) Representation of two MBP-GSDMB_C Arg299:Ser306 molecules in the asymmetric unit. The cylinders depict α-helices. MBP is colored gray, and GSDMB_C colors are ramped from blue at the N terminus to red at the C terminus. Core α-helices that form the α-helix bundle are numbered α5 to α11. A short α-helix within the polymorphism loop connecting the α7 and α8 helices is labeled α′. An additional unlabeled 1-turn α-helix within the polymorphism loop is present only in structures of Ser306-containing variants. (*B*) Stereoscopic representation of the GSDMB_C Arg299:Ser306 variant, in the same coloring scheme as in *A*. Two disordered regions, the interdomain linker before α5 and the loop between α10 and α11, are depicted in dotted lines.

of linker conformational order/disorder correlates with different intermolecular contacts. Only three molecules in the MBP-GSDMB_C Gly299:Pro306 structure have well-resolved electron density over the entire linker region (molecules B, E and J; PDB ID code 5TJ2). The markedly different conformations of these resolved linkers underscore the apparent flexibility of this region, which would be a useful property for regulating the activity of GSDMB by possibly altering the relative orientation of the two domains.

The flexible linker is followed by the GSDMB_C core structure (Asn248–Pro406), exhibiting a bundle of 7 α-helices (α5–α11) (Figs. 1 and 2). The helical core contains another disordered loop connecting the last two helices, α10 and α11 (Glu367–Tyr382), as depicted by a red dotted line in Fig. 2*B*. Again, although two versions of this loop could be fully traced in the electron density of the MBP-GSDMB_C Gly299:Pro306 structure (molecules A and C; PDB ID code 5TJ2), these defined loops contain no secondary structure elements and adopt different conformations. Another loop within the core GSDMB_C connects the α7 and α8 helices (Arg299–Val322) shown at the bottom left in Fig. 2. This loop contains the two polymorphism amino acids at positions 299 and 306. All 16 versions of this loop contain a five-residue α-helix (labeled α′), spanning residues Pro309 to Ser313. However, molecules that contain a Ser at position 306 (MBP-GSDMB_C Arg299:Ser306 and Gly299:Ser306) adopt an additional four-residue helical turn at residues Met303–Ser306 between the α7 and α′ helices. Loops that contain a Pro at position 306 do not form this helical turn.

The seven-helix bundle topology of GSDMB_C and the related Gsdma3 topology (PDB ID code 5B5R) are unusual. A DALI search (36) revealed a single structure exhibiting the same topology: that of the cytoplasmic domain of a putative membrane protein from *Clostridium difficile* 630 (PDB ID code 3KMI, determined by the Midwest Structural Genomic Consortium). The DALI program calculates a Z-score of 6.5 and a C^{α} position rmsd value of 4.5 Å for 112 of the 167 aligned residues, with 13% amino acid sequence identity (Fig. 3). Despite the common topologies, the superposed structures show substantial differences (Fig. 3). The helices of the GSDMB_C core are much shorter, two loops are significantly longer, and GSDMB_C has an additional N-terminal α-helix (α5, colored gray in Fig. 3). The Pfam database annotates this structure (PDB ID code 3KMI)

as belonging to the C-terminal domain of the ArAE_1_C aromatic acid exporter family (Transporter Classification Database; ref. 37). *Escherichia coli* YhcP, a member of the ArAE_1_C family, has been characterized as an efflux pump that alleviates toxic effects of p-hydroxybenzoic acid on the metabolic balance of *E. coli* (38). Taken together, the structural relationship seems too remote to derive conclusions about the function of GSDMB.

Impact of Amino Acid Residues 299 and 306 on the Structure. Of the human genomes sequenced by the 1000 Genomes Project (33), the *GSDMB* polymorphisms encoding the alleles containing either Gly299:Pro306 or Arg299:Ser306 are present at ∼50% frequency in the general population (22). The *GSDMB* SNPs associated with inflammatory disease risks encode the Arg299:Ser306 variant. Fig. 4 compares the conformations of the loop region that carries the pairs of polymorphism residues. Loops containing Pro306 exhibit a wide range of backbone conformations (Fig. 4*A*). In contrast, loops containing Ser306 (MBP-GSDMB_C Arg299:Ser306 and Gly299:Ser306) exhibit a helical turn preceding Ser306 and a tight range of loop conformation (Fig. 4*B*). The backbone conformation close to residue 299 is similar, regardless of the presence of a glycine or an arginine in all 16 GSDMB_C molecules (Fig. 4*B*). However, the presence or absence of a positive charge, when position 299 is occupied by an Arg or a Gly, would impact the surface electrostatics in the vicinity. Modeling a Pro in the place of Ser at position 306 illustrates why a proline side chain cannot be accommodated in the context of the preceding helical turn (Fig. 4*C*). The model shows short contacts (<1.5 Å) between both the C^{γ} and C^{δ} atoms of the proline to the backbone oxygen atom of Met303. Apparently, the accommodation of the proline side chain at position 306 is accompanied by the loop adopting extensive conformational flexibility (Fig. 4*A*).

Unlike monogenic diseases, caused by high-penetrance SNPs in single genes, complex-trait diseases are associated with multiple

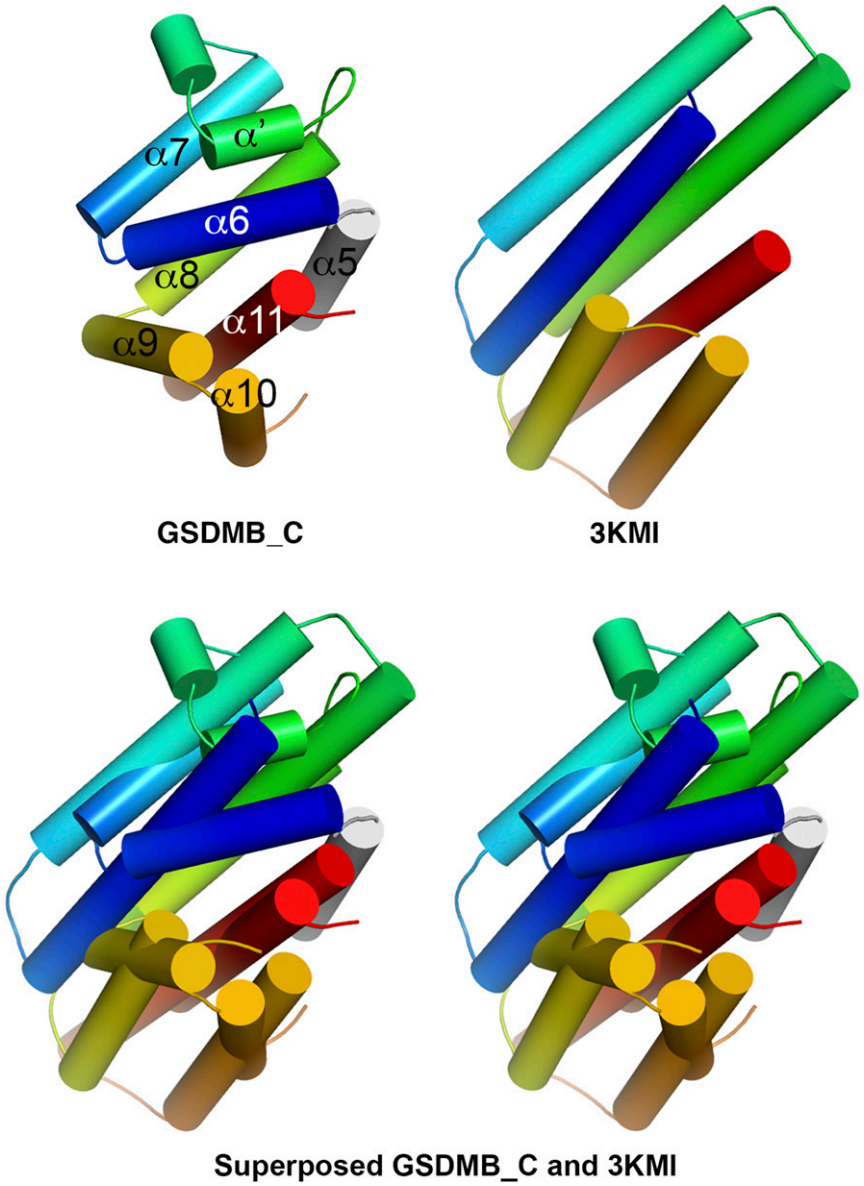

Fig. 3. Structural comparison of GSDMB_C and the cytoplasmic domain of a putative membrane protein from *C. difficile* 630 (PDB ID code 3KMI). Helices are shown as cylinders. Colors are ramped from blue at the N terminus to red at the C terminus, except that the first GSDMB_C helix, α5, missing in the 3KMI structure, is colored gray. (*Top*) Side-by-side view of the two structures. (*Bottom*) Stereoscopic view of the superposed structures.

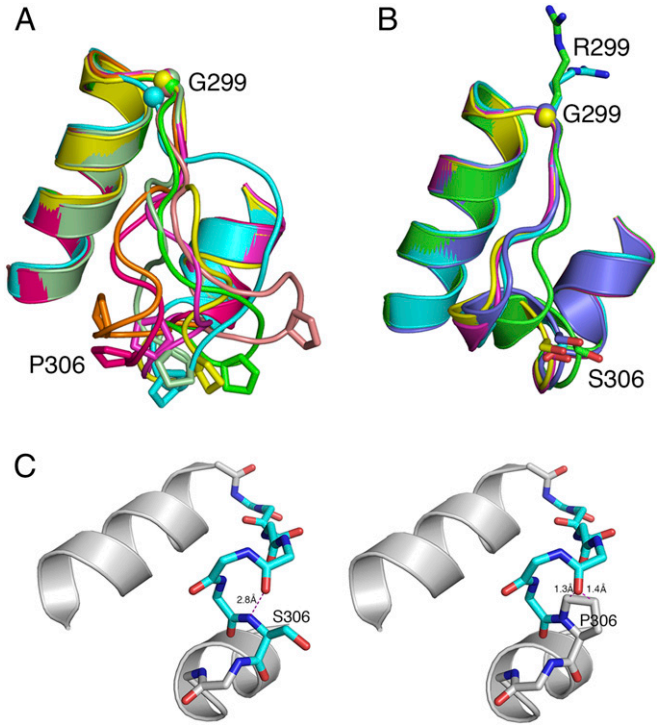

Fig. 4. Alternative conformations of the GSDMB polymorphism loop. The superposed loops are shown in different colors. The superpositions were obtained from the least-squared alignment of the flanking helices. The polymorphism residues are as indicated. (*A*) MBP-GSDMB_C Gly299:Pro306; Gly299 is shown as a sphere. (*B*) MBP-GSDMB_C Arg299:Ser306 (disease-associated variant) and Gly299:Ser306. (*C*) The environment of Ser306 in the structure of MBP-GSDMB_C Arg299:Ser306 and a model of a proline, built in the context of that environment. The proline side chain clashes with the carbonyl oxygen of Met303, and thus a proline cannot be accommodated while maintaining the helical conformation.

low-penetrance SNPs in multiple genes. Because of linkage disequilibrium, most of the SNPs present in a genome are actually not disease-causative. The GWAS results highlighted the complexity of SNP patterns emerging from the genomic sequences of large populations and underscored the challenges of identifying truly disease-causative SNP candidates. The current study provides structural perspective for possible disease risk mechanisms attributed to candidate SNPs. In addition to the strikingly different conformations of the GSDMB Arg299:Ser306 and Gly299:Pro306 containing loops, a change from a glycine to an arginine at position 299 alters the charge distribution on the protein surface. One or both of these changes may contribute to the susceptibility of individuals to develop inflammatory bowel diseases and asthma through one of the following molecular mechanisms: (*i*) The difference in the inherent stability of the GSDMB variants and/or their susceptibility to cellular protein degradation machinery may lead to different cellular concentrations, which in turn may affect disease risk; (*ii*) different loop conformations and surface charges of the two GSDMB variants may lead to altered interactions between the N- and C-terminal domains, thus affecting protein activity; and (*iii*) the two GSDMB variants may interact differently with protein partners, such as the reported HSP90β and fatty acid synthetase (8).

GSDMB Stability and Caspase Cleavage Profile. To investigate these possible mechanisms, circular dichroism was used to measure the thermal stability of the GSDMB_C variants (encompassing amino acids Asp244–Ser411). The CD spectra of both GSDMB_C Arg299:Ser306 and Gly299:Pro306 variants show no thermal unfolding transition upon heating from 22 °C to 90 °C. This result reveals a highly stable C-terminal domain and indicates that the polymorphism residues at positions 299 and 306 do not affect protein stability at physiological temperature. Thus, GSDMB stability is not a likely mechanism underlying the complex-trait inflammatory disease risk.

Shi et al. have shown that GSDMB is not a substrate for the inflammatory caspases 1 and 4/5/11 whereas GSDMD is cleaved by these caspases in the interdomain linker (29). We investigated whether GSDMB is a substrate of the human apoptotic caspases and found that His_6-GSDMB, MBP-GSDMB, and MBP-GSDMB_N are substrates of the apoptotic executioner caspases 3, 6, and 7 (Fig. 5). The higher molecular weight cleavage products from His_6-GSDMB and MBP-GSDMB_N are recognized by the anti-GSDMB_C and anti-MBP antibodies, respectively (Fig. 5, *Bottom*). The molecular weights of the proteolytic fragments indicate that the caspase recognition site is in the N-terminal domain of GSDMB and not in the interdomain linker region. N-terminal sequencing of the C-terminal fragment from a caspase-3 cleavage reaction revealed amino acids $_{92}$STGELIVRLP$_{101}$ (Fig. 1), and thus the cleavage site is after $_{88}$DNVD$_{91}$. Interestingly, the CaspDB lists this site with the highest caspase cleavage probability (39). Thus, human apoptotic executioner caspases did not generate an entire GSDMB N-terminal domain, analogous to the pyroptotic N-terminal domain of GSDMD.

The loop containing the polymorphism amino acids also contains another predicted caspase recognition site, $_{304}$EDPD$_{307}$, albeit with a probability score of 0.803. All four MBP-GSDMB_C variants (Gly299:Pro306, Arg299:Ser306, Gly299:Ser306, and Arg299:Pro306) were digested with caspases 1 to 3 and 6 to 10, but none was cleaved. The functional significance of caspase 3/6/7 cleavage at an internal GSDMB's N-terminal domain site and its impact on the protein activity are currently unknown.

GSDMB_N Binds Phosphoinositides and Sulfatide. Ding et al. first discovered that the N-terminal domains of Gsdma3, GSDMA, and GSDMD bind phospholipids (25). The C-terminal domains inhibit phospholipid binding to the full-length proteins, but not

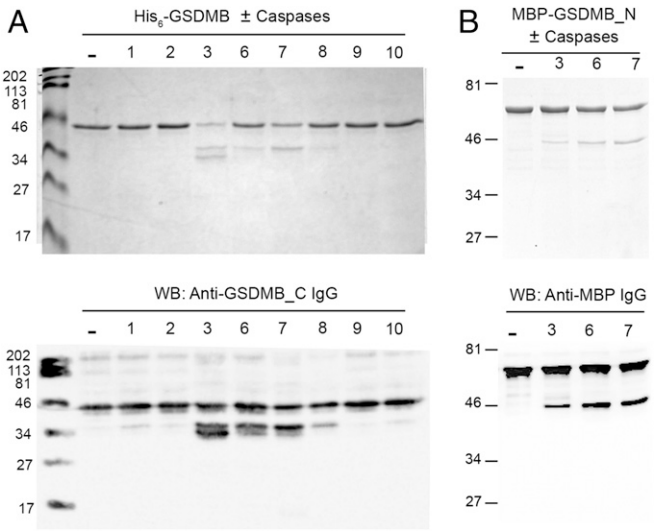

Fig. 5. GSDMB is a substrate of apoptotic, executioner caspase 3, 6, and 7. In vitro cleavage of (*A*) His_6-GSDMB by recombinant human caspases 1 to 3 and 6 to 10 and (*B*) MBP-GSDMB_N by recombinant human caspases 3, 6, and 7. The cleavage products are separated on 14% (wt/vol) SDS/PAGE (*Top*) and immunoblotted with anti-GSDMB mAb and goat anti-Mouse HRP conjugate (*A*, *Bottom*) and with anti-MBP conjugated to HRP mAb (*B*, *Bottom*).

to noncovalent N+C complexes. The identified phospholipids were components of the cell membrane's inner leaflets, including monophosphoinositides [PtdIns(3)P, PtdIns(4)P, and PtdIns(5)P], bisphosphoinositides [PtdIns(3,4)P_2, PtdIns(3,5)P_2, and PtdIns(4,5)P_2], triphosphoinositide [PtdIns(3,4,5)P_3], and cardiolipin [1,3-bis(sn-3′-phosphatidyl)-sn-glycerol]. Subsequent reports confirmed the binding of GSDMD_N to PtdIns(4)P, PtdIns(3,4)P_2, phosphatidic acid, and cardiolipin, and weakly to phosphatidylserine (32). Because cardiolipin is a component of the inner leaflet of mitochondrial membrane, the binding data substantiated previous results that Gsdma3 is transported into the mitochondria to disrupt mitochondrial membranes (26, 27) although mitochondrial localization was not reported for GSDMD. For GSDMD, phospholipid binding enables higher order oligomerization of the GSDMD N-terminal domain in the lipid bilayer and formation of ring structure-like pores to disrupt membrane structure. These data also imply either that the interfaces between the two domains of intact Gsdma3, GSDMA, and GSDMD overlap with the phospholipid binding sites on the respective N-terminal domains or that the GSDMs' C-terminal domains induce protein conformations in the vicinity of the binding sites that impede lipid binding.

We screened the lipid binding activity of MBP-GSDMB_N, MBP-GSDMB_C, full-length MBP-GSDMB, and His_6-GSDMB using the nitrocellulose membrane immobilized with phosphoinositides, membrane lipids, and sphingolipids. The GSDMBs containing the N-terminal domain bound mono-, bis-, and triphosphoinositides (Fig. 6). Weaker binding activities were also observed for phosphatidic acid, phosphatidylglycerol, sulfatide (3-*O*-sulfogalctosylceramide), and cardiolipin. In contrast, all four MBP-GSDMB_C variants and His_6-MBP control did not bind any lipids. Thus, the lipid-binding activity of GSDMB is also located in its N-terminal domain. Additional experiments with the lipid arrays, nitrocellulose membrane spotted with varied lipid amounts, confirmed most but not all of the initial binding activities of GSDMB and highlighted variability in the lipid-binding affinities of the full-length and N-terminal domain of GSDMB (Fig. 6*B*). Strikingly, unlike other gasdermins, the presence of the GSDMB C-terminal domain in the full-length protein did not prevent phospholipid binding. This finding and the affinity for sulfatide, not for cardiolipin, distinguish GSDMB from Gsdam3/GSDMA and GSDMD. The lipid-binding activity of intact GSDMB could be due to either that (*i*) the interdomain interaction between the N- and C-terminal domains of GSDMB is weaker than that of the other gasdermins or (*ii*) that the phospholipid binding site on the GSDMB N-terminal domain is not in the vicinity of the interdomain interface, as suggested for GSDMA (25). Currently there is no evidence that a stable N-terminal domain is generated from a proteolytic cleavage of GSDMB. Thus, unlike GSDMA/Gsdma3 and GSDMD, a pyroptotic activity of the recombinant GSDMB N-terminal domain, as reported by Ding et al. (25), may be decoupled from its phospholipid-binding activity because the full-length GSDMB is noncytotoxic despite similar lipid binding properties.

Liposome-binding experiments were performed to confirm that the unique sulfatide binding to GSDMB_N is not an artifact due to unspecific charge–charge interactions. These studies showed that, indeed, the N-terminal domain bound liposomes containing sulfatide whereas the C-terminal domain did not.

GSDMB May Have a Different Interdomain Interaction than That of Gsdma3. To gain insights into the lipid-binding property of the full-length GSDMB, we compared the structures of the GSDMB_C and Gsdma3 (25). The topology of the shared seven-helix bundle is conserved, and the rmsd of 113 Cα positions shared between the C-terminal domains of GSDMB and Gsdma3 is 2.3 Å (Fig. 7). However, examination of the superposed structures suggests that there are important differences that may lead to a different interdomain orientation of GSDMB compared with Gsdma3 (and perhaps also GSDMA and GSDMD), which may explain why the C-terminal domain of GSDMB does not inhibit lipid binding. First, the conformations of the GSDMB loop containing the polymorphism residues and that of Gsdma3 are entirely different (colored red in Fig. 7). Second, another region within the GSDMB and Gsdma3 C-terminal domains is strikingly different (colored blue in Fig. 7). The GSDMB_C flexible loop (Met366–Tyr382) that connects the last two helices (α10–α11) has a counterpart segment in Gsdma3, which is 33 aa longer (Pro384–Asp433, colored blue in Fig. 7). The Gsdma3 Pro384–Asp433 segment links α10 and α12 helices and forms a subdomain comprising an α-helix (α11) and a 3 β-stranded sheet (β12–β14) (Fig.1). Notably, helix α11 of Gsdma3 extends the number of helices of its C-terminal helix bundle to eight. This Gsdma3 subdomain interacts with Gsdma3 α4 (Pro179–Asn187) within a largely disordered N-terminal domain loop (Thr168–Asn193) that has been shown by site-directed mutagenesis (replacement of Gsdma3 Leu184 or GSDMD Leu192 with an Asp) to be involved in membrane disruption (25). For the shorter GSDMB loop (Met366–Tyr382) to regulate the interaction of the N-terminal domain with cellular membranes, the interdomain orientation must change.

Third, three Gsdma3 N-terminal domain segments interact with the C-terminal domain (colored magenta in Fig. 7): the N-terminal α1 helix (Met1–Asn16), an Ω-loop connecting β1 and β2 (Lys42–Arg52), and the structurally defined α4 (Pro179–Gln187) of the otherwise disordered membrane-disrupting loop (Thr168–Asn193). By comparison, the predicted Ω- and membrane-disrupting loops in the N-terminal domain of GSDMB are shorter by 3 and 4 aa (Fig.1), and they cannot adopt the same conformations as those observed in the Gsdma3 structure. To accommodate all these changes, the mode of interactions between the N- and C-terminal domains of GSDMB and Gsdma3 are likely to be different.

Finally, of the six alternative splice variants of the GSDMB, five have interdomain linkers that vary in length and sequence. These variations are likely to modulate the mode of interdomain interactions and perhaps also the GSDMB affinities to lipids and protein partners. Indeed, the 394-aa-long GSDMB splice variant (NCBI NP_061000.2, GSDMB-2) exhibited different activities than the 403-aa splice variant (NCBI NP_001035936.1, GSDMB-1). Overexpression of the GSDMB-2 variant led to increased activation of Rac-1 and Cdc-42 and metastatic burden compared with overexpression of GSDMB-1. In addition, although both GSDMB splice variants interacted with HSP90, only GSDMB-2 relied on the chaperone for its stability (8). We speculate that the longer or shorter linker segments, as well as the different linker amino acid sequences of splice variants, may modulate protein activity and/or direct the protein to different subcellular compartments and cell fates.

Implications for GSDMB's Function in Health and Disease. The structures reported here reveal the conformational and surface electrostatic differences that accompany the GSDMB_C amino acid replacements encoded by SNPs linked to increased risk of developing complex-trait inflammatory diseases, such as asthma, Crohn's, and ulcerative colitis. The GSDMB C-terminal domain does not inhibit the lipid-binding activity of its N-terminal domain, as reported for other gasdermins. Therefore, amino acid replacements in the GSDMB C-terminal domain offer a nuanced mechanism to regulate protein activity. It is currently unknown whether the C-terminal domain modulates the lipid selectivity and/or binding affinity by directly interacting with the N-terminal domain or by associating with a partner protein such as HSP90β or fatty acid synthetase. In addition to phosphoinositides, the binding of sulfatide to GSDMB seems to be unique and was not observed for GSDMA, Gsdma3, and GSDMD (25, 32). Sulfatide is synthesized in the Golgi apparatus from galactosylceramide and then is distributed to the extracellular leaflet of myelin, to

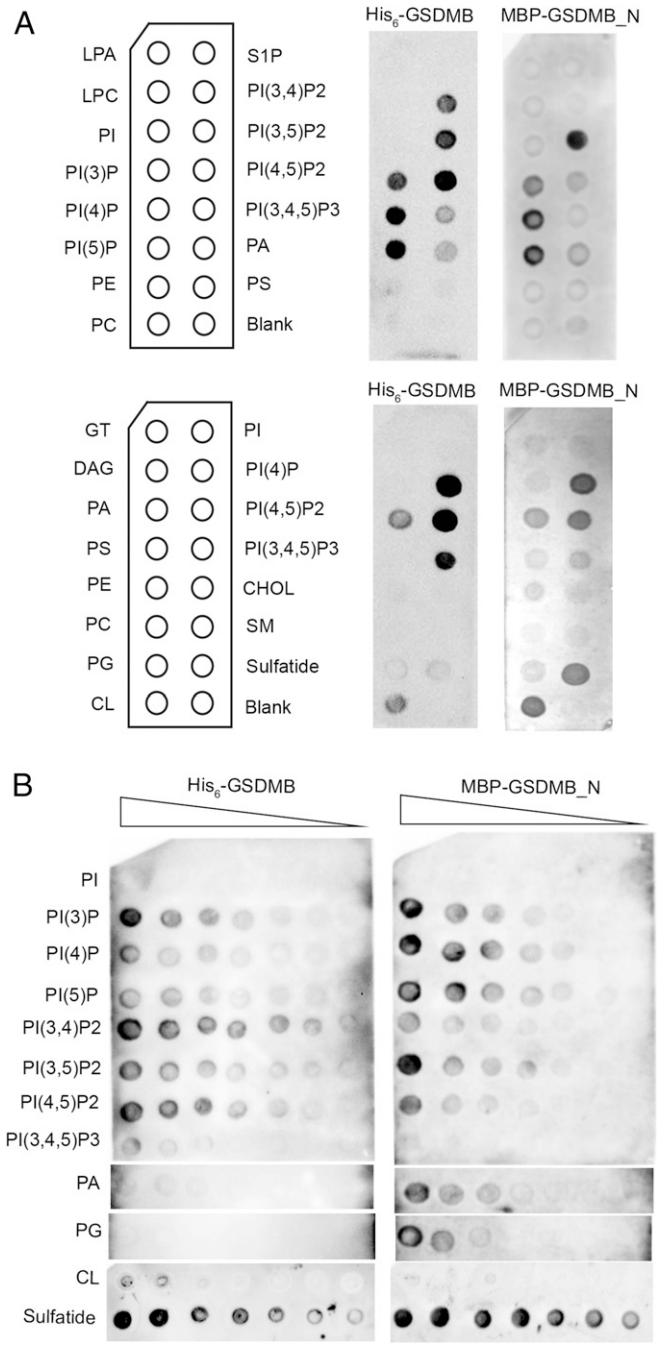

Fig. 6. Protein-lipid overlay assay shows the binding of phosphatidylinositides and sulfatide to His_6-GSDMB and MBP-GSDMB_N. (*A*) His_6-GSDMB or MBP-GSDMB_N were incubated with phospholipid (*Left*) or membrane lipid (*Right*) strips. Then, 100 pmol of each lipid was immobilized on nitrocellulose membrane. Schematics of lipid strip templates are shown with lipid labels. CHOL, cholesterol; DAG, diacylglycerol; GT, triglyceride; LPA, lysophosphatidic acid; LPC, lysophosphocholine; PC, phosphatidylcholine; PE, phosphatidylethanolamine; PS, phosphatidylserine; PtdIns, phosphatidylinositol; PtdIns(3)P, phosphatidylinositol-3-phosphate; PtdIns(4)P, phosphatidylinositol-4-phosphate; PtdIns(5)P, phosphatidylinositol-5-phosphate; PtdIns(3,4)P_2, phosphatidylinositol-3,4-bisphosphate; PtdIns(3,5)P_2, phosphatidylinositol-3,5-bisphosphate; PtdIns(4,5)P_2, phosphatidylinositol-4,5-bisphosphate; PtdIns(3,4,5)P_3, phosphatidylinositol-3,4,5-triphosphate; SM, sphingomyelin; S1P, sphingosine-1-phosphate; sulfatide, 3-sulfogalactosylceramide. (*B*) His_6-GSDMB (2 μg/mL) and MBP-GSDMB_N (2.6 μg/mL) were incubated with varying amounts of immobilized phosphoinositides, phosphatidic acid (PA), phosphatidylglycerol (PG), cardiolipin (CL), and sulfatide on nitrocellulose membrane. Phosphoinositides, PA, and PG concentrations are 100, 50, 25, 12.5, 6.25, 3.75, and 1.56 pmol. Cardiolipin and sulfatide concentrations are 1,000, 800, 600, 400, 200, 100, and 50 pmol.

the apical membrane of epithelial cells, and also to the lysosome for degradation. Lipodomic analysis showed a dramatic increase in sulfatide level, with progression of epithelium polarization, a process that protects the integrity of the epithelial cell barrier (40). Elevated levels of sulfatide are documented in many cancers. Abundant sulfatide on the surface of cancer cells may serve as a native ligand for P-selectin, a protein that promotes cell migration and metastasis (41). Sulfatide also stimulated phosphorylation of transcription factor Sp1 in hepatocellular carcinoma cells through Erk1/2 signaling, which in turn increased expression of the integrin αV subunit, another protein involved in metastasis (42). In ulcerative colitis, the mucosa is enriched with type II NKT cells, and sulfatide binds to these cells to induce production of IL-13, which mediates epithelial cell cytotoxicity (43). In asthma, transgenic mice overexpressing the human GSDMB developed asthmatic symptoms, and an overexpression of GSDMB in bronchial epithelial cells induced the expression of 5-lipoxygenase, which in turn induced TGF-β1 expression (44). 5-Lipoxygenase converts arachidonic acid and the omega-3 fatty acid icosapentaenoic acid into the signaling lipids leukotrienes, and sulfatide inhibits the enzyme (45). Currently, cytoplasmic protein(s) that specifically transport sulfatide between cellular compartments have not been identified. Could the GSDMB be a part of the epithelial cell transport system that targets sulfatide to the plasma membrane? Then, overexpression of GSDMB might be responsible for higher sulfatide levels on the apical surface of epithelial cells. For the GSDMB SNPs associated with inflammatory bowel diseases and asthma, if expression of the GSDMB R299:S306 SNP variant protein leads to aberrant sulfatide transport, this perturbation might compromise the integrity of the epithelial cell barrier and/or promote inflammatory processes.

In conclusion, we report molecular properties that distinguish GSDMB from other GSDMs, providing evidence to explain the different biology associated with the oncogenic GSDMB and the apoptotic GSDMA, GSDMC, and GSDMD. First, intact, full-length GSDMB binds signaling lipids in contrast to other GSDMs, whose C-terminal domains inhibit lipid binding, and only their free N-terminal domains can bind lipids, form pores, and kill cells. Second, we discovered that GSDMB binds sulfatide, but not cardiolipin, in contrast to other GSDMs, which exhibit the reverse binding specificity. The reported involvement of sulfatide on the surface membrane of epithelial cells in some cancers and complex trait inflammatory disease suggests that GSDMB may function in sulfatide cellular transport. In addition, GSDMB and other GSDMs also bind phosphoinositides. The biological implications of these phosphoinositide-binding activities are currently unknown and warrant further investigations. Third, the structures of the GSDMB C-terminal domain show that the SNPs associated with complex trait inflammatory disease alter the flexibility and charge of a surface loop, properties that might be responsible for activity modulation. It remains to be discovered whether the altered loop properties exert an intramolecular effect (i.e., via an interaction with GSDMB's N-terminal domain) or an intermolecular effect (i.e., via an unknown protein–protein interaction). Nevertheless, the structure analysis offers a potential disease mechanism in support of GWAS data that implicated GSDMB polymorphism in disease risk.

Materials and Methods

Cloning, Expression, and Protein Purification. The human *GSDMB* gene was amplified from a cDNA clone (ID 5205060; Open Biosystems, Inc.) and was ligated into the NotI and NheI sites in the pMALX(E) vector (kindly provided by Lars C. Pedersen, National Institute of Environmental Health Sciences, Research Triangle Park, NC) for expression in *E. coli*. The maltose-binding

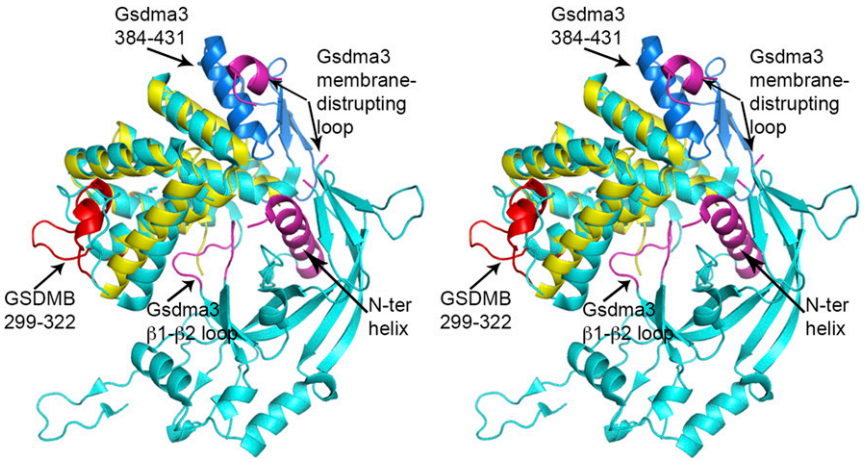

Fig. 7. Comparison of GSDMB_C and Gsdma3 structures. Stereoscopic view of the superposed structures. GSDMB_C is colored in yellow and Gsdma3 is colored in cyan. The α7 to α8 GSDMB loop carrying the polymorphism residues is colored in red. The Gsdma3 region corresponding to the flexible GSDMB loop connecting α11 and α12 is colored in blue. Regions of the Gsdma3 N-terminal domain that interact with the C-terminal domain are colored in magenta.

protein (MBP) contains five mutations, D82A/K83A/E172A/N173A/K239A, and a 3-alanine extension at the C terminus. Point mutations in GSDMB_C were introduced using the QuikChange mutagenesis protocol (Stratagene) and were confirmed by sequencing. The recombinant MBP-GSDMB_C protein spans Lys1 to Ala370 of MBP and Met220 to Ser411 of GSDMB_C. *E. coli* BL21*(DE3) cells transformed with plasmid were grown in LB medium containing 0.1 mg/mL ampicillin for 16 h at 37 °C. The culture was diluted 1:100 into fresh LB-Amp medium, and the cells were grown at 37 °C to a density of OD_{600} ~0.6. The incubation temperature was reduced to 22 °C before the addition of 0.4 mM isopropyl β-D-1-thiogalactopyranoside (IPTG), and the cells were grown for 16 h. Cells transformed with the MBP-GSDMB_N gene (MBP fused to GSDMB Phe2-Ilu226) were grown at 22 °C to a density of OD_{600} ~0.2, before the addition of 1 mM IPTG, and were grown for 16 h at 15 °C. For the MBP-GSDMB_N and MBP-GSDMB_C fusion proteins, cells resuspended in 50 mM Tris·HCl (pH 8.0), 0.1 M NaCl, 1 mM ethylene-diamine-tetra-acetic acid (EDTA), 10% (vol/vol) glycerol, 0.17 mg/mL lysozyme, and 3.3 units/mL benzonase (Novagen) were lysed by sonication. The cell lysate was centrifuged for 1 h at 23,700 × *g* at 4 °C, and the soluble fraction was applied onto an amylose column (NEB), equilibrated in 50 mM Tris·HCl (pH 8.0), 0.10 M NaCl, 0.5 mM EDTA. After washing the column, the bound protein was eluted with the above buffer containing 10 mM maltose. The protein was further purified using size exclusion chromatography with a Sephacryl S200 column equilibrated in 50 mM Hepes (pH 7.3), 0.1 M NaCl, 0.02% NaN_3, 10 mM maltose at 4 °C. Full-length MBP-GSDMB (MBP fused to GSDMB Phe2-Ser411) was coexpressed in the presence of chaperone proteins, GroEL/GroES, following the manufacturer protocol (TAKARA BIO Inc.). *E. coli* BL2*(DE3) cells transformed with expression vectors for MBP-GSDMB and GroEL/GroES were grown at 37 °C in the presence of 50 μg/mL ampicillin, 20 μg/mL chloramphenicol, and 0.5 mg/mL L-arabinose to a density of OD_{600} ~0.8, before the addition of 0.2 mM IPTG, and then grown for 4 h. MBP-GSDMB was copurified from an Amylose affinity column with GroEL/GroES. The chaperones were removed by precipitation of MBP-GSDMB with 1.8 M ammonium sulfate. MBP-GSDMB was further purified by a Superdex 200 size exclusion column. For the His_6-GSDMB protein, *GSDMB* was cloned into the baculovirus transfer vector, pVL1393 (BD Biosciences), with an N-terminal His_6-tag and seven-residue tobacco etch virus protease cleavage site. The engineered pVL1393 was cotransfected with Sapphire Baculovirus DNA (Allele Biotechnology) into Sf9 cells (Gibco). The recombinant baculovirus was used to transfect Sf9 cells grown in SF-900 II SFM (Gibco) at 27 °C. Cells were harvested 4 d posttransfection and lysed in 150 mL of 10 mM Tris·HCl (pH 7.5), 0.15 M NaCl, 1% (vol/vol) Nonidet P-40, 1 mM DTT, and protease inhibitor mixture. The lysate was centrifuged at 212,795 × *g* for 1 h, and the supernatant was applied to an Ni^{2+}-NTA column (Qiagen). His_6-GSDMB was eluted with the above buffer containing 10 to 250 mM imidazole and further purified using a phenyl Sepharose column. The protein concentrations were determined at 280 nm wavelength with a calculated extinction coefficient of 74,955 $M^{-1}{\cdot}cm^{-1}$, for MBP-GSDMB_C, 86,415 $M^{-1}{\cdot}cm^{-1}$ for MBP-GSDMB_N, 95,020 $M^{-1}{\cdot}cm^{-1}$ for MBP-GSDMB, and 30,160 $M^{-1}{\cdot}cm^{-1}$ for His_6-GSDMB.

Crystallization, Data Collection, and Structure Determination. Crystals of MBP-GSDMB_C Gly299:Pro306 were obtained at room temperature using the vapor diffusion method with 3-μL drops comprising equal volumes of protein (containing 10 mM maltose) and reservoir solution containing 2.1 M sodium malonate (pH 6). The MBP-GSDMB_C Arg299:Ser306 variant and Gly299:Ser306 variant crystals were obtained using reservoir solutions of 2.2 M sodium malonate (pH 6) and 9 mM hexamine $CoCl_3$ or 10 mM EDTA, respectively. For data collection, crystals were transferred to 2.6 M sodium malonate (pH 6) and 10 mM maltose, supplemented with either 9 mM hexamine $CoCl_3$ or 10 mM EDTA, and flash-cooled in liquid nitrogen. Diffraction data were collected at the General Medicine and Cancer Institute (GM/CA, 23ID-B) and the Structural Biology Center (SBC, 19ID) Collaborative Access Team beamlines at the Advanced Photon Source (Argonne National Laboratory). Diffraction data were processed with MOSFLM (46). The structure was determined by molecular replacement using the program PHASER (47) with the MBP structure (PDB ID code 3H4Z) as the search model for the MBP-GSDMB_C Arg299:Ser306 variant structure. The MBP-GSDMB_C Arg299:Ser306 structure then served as the search model for the two additional structures. The phase improvement program PARROT (48) was used to improve the initial electron density maps. Structure refinement and model building were performed with the program REFMAC5 (49) and the interactive computer graphics program COOT (50). Figures were prepared with PyMOL (The PyMOL Molecular Graphics System; Schrödinger, LLC) and ESPript 3 (51).

Protein Lipid Overlay Assay. Nitrocellulose strips and arrays of phosphoinositides (PIPs), membrane lipids, sphingophospholipids (Echelon Biosciences), and nitrocellulose arrays of cardiolipin and sulfatide (prepared as described) (52) were blocked in Tris-buffered saline containing 0.1% (vol/vol) Tween 20 and 3% fatty acid-free BSA (TBST-BSA; Sigma) for 1 h at room temperature. The membranes were incubated with 2 to 3 μg/mL MBP-GSDMB, MBP-GSDMB_N, MBP-GSDMB_C, or His_6-MBP in TBST-BSA buffer overnight at room temperature. After three washes with TBST-BSA, the membranes were blotted with anti-MBP monoclonal antibody conjugated to HRP, or with anti-GSDMB C-terminal monoclonal antibody and goat anti-mouse IgG HRP conjugate. The blots were visualized using Supersignal West Pico enhanced chemiluminescence substrate.

For liposome-binding assays, liposomes containing 4:1 molar ratio egg L-α-phosphatidylcholine and porcine brain sulfatide (Avanti Polar Lipids) were prepared as previously described (53). MBP-GSDMB_N, MBP_GSDMB_C or GSDMB_C were incubated with 0.5 to 1 mM liposomes for 30 min at 22 °C in an 80-μL reaction volume. The samples were centrifuged in a Beckman TL-100 μL tracentrifuge for 20 min at 4 °C at 128,000 × *g*. The supernatant was collected. The pellet was washed with 100 μL of buffer [100 mM NaCl, 20 mM Hepes/NaOH (pH 7.5), and 0.02% sodium azide] and recentrifuged, and buffer was added to obtain the same volume as that of the supernatant. The proteins in the supernatant and pellet fractions were analyzed by SDS/PAGE and Coomassie blue staining.

In Vitro Caspase Cleavage Assay. Active human recombinant caspases 1, 2, 3, 6, 7, 8, 9, and 10 were purchased from BioVision. Approximately 1 μM His_6-GSDMB, or 3.5 μM MBP-GSDMB, or 1.6 μM MBP-GSDMB_N, or 1.3 μM MBP-GSDMB_C was

incubated with 1 unit of active caspases at 37 °C for 2 h in a 25-μL buffer [50 mM Hepes (pH 7.3), 50 mM NaCl, 10 mM EDTA, 0.1% CHAPS, 10 mM DTT, 5% glycerol]. The cleavage products were resolved by 14% (wt/vol) SDS/PAGE under denaturing conditions, and Western analyses were conducted as described above. For the mapping of the caspase cleavage site on GSDMB, a pET21b vector containing the Caspase 3 gene (kindly provided by A. Clay Clark, University of Texas at Arlington, Arlington, TX) was purified as previously described (54).

ACKNOWLEDGMENTS. We thank Drs. John Moult and Lipika Pal for advice and useful discussions regarding bioinformatics information. We thank Drs. Gema Moreno-Bueno and David Sarrió, Autonomous University of Madrid, Madrid, for the generous gift of the anti-GSDMB_C monoclonal antibody. We thank the staff at the General Medicine and Cancer Institute (GM/CA, 23ID-B) and the Structural Biology Center (SBC, 19ID) Collaborative Access Team beamlines at the Advanced Photon Source for help with X-ray data collection. This work was supported by National Institutes of Health Grant R01-GM102810.

1. Tamura M, et al. (2007) Members of a novel gene family, Gsdm, are expressed exclusively in the epithelium of the skin and gastrointestinal tract in a highly tissue-specific manner. *Genomics* 89(5):618–629.
2. Carl-McGrath S, Schneider-Stock R, Ebert M, Röcken C (2008) Differential expression and localisation of gasdermin-like (GSDML), a novel member of the cancer-associated GSDMDC protein family, in neoplastic and non-neoplastic gastric, hepatic, and colon tissues. *Pathology* 40(1):13–24.
3. Komiyama H, et al. (2010) Alu-derived cis-element regulates tumorigenesis-dependent gastric expression of GASDERMIN B (GSDMB). *Genes Genet Syst* 85(1):75–83.
4. Saeki N, et al. (2007) GASDERMIN, suppressed frequently in gastric cancer, is a target of LMO1 in TGF-beta-dependent apoptotic signalling. *Oncogene* 26(45):6488–6498.
5. Saeki N, Kuwahara Y, Sasaki H, Satoh H, Shiroishi T (2000) Gasdermin (Gsdm) localizing to mouse Chromosome 11 is predominantly expressed in upper gastrointestinal tract but significantly suppressed in human gastric cancer cells. *Mamm Genome* 11(9):718–724.
6. Saeki N, et al. (2009) Distinctive expression and function of four GSDM family genes (GSDMA-D) in normal and malignant upper gastrointestinal epithelium. *Genes Chromosomes Cancer* 48(3):261–271.
7. Sun Q, et al. (2008) Expression of GSDML associates with tumor progression in uterine cervix cancer. *Transl Oncol* 1(2):73–83.
8. Hergueta-Redondo M, et al. (2014) Gasdermin-B promotes invasion and metastasis in breast cancer cells. *PLoS One* 9(3):e90099.
9. Watabe K, et al. (2001) Structure, expression and chromosome mapping of MLZE, a novel gene which is preferentially expressed in metastatic melanoma cells. *Jpn J Cancer Res* 92(2):140–151.
10. Bisgaard H, et al. (2009) Chromosome 17q21 gene variants are associated with asthma and exacerbations but not atopy in early childhood. *Am J Respir Crit Care Med* 179(3):179–185.
11. Bouzigon E, et al. (2008) Effect of 17q21 variants and smoking exposure in early-onset asthma. *N Engl J Med* 359(19):1985–1994.
12. Flory JH, et al. (2009) 17q12-21 variants interact with smoke exposure as a risk factor for pediatric asthma but are equally associated with early-onset versus late-onset asthma in North Americans of European ancestry. *J Allergy Clin Immunol* 124(3):605–607.
13. Galanter J, et al. (2008) ORMDL3 gene is associated with asthma in three ethnically diverse populations. *Am J Respir Crit Care Med* 177(11):1194–1200.
14. Granell R, et al. (2013) Examination of the relationship between variation at 17q21 and childhood wheeze phenotypes. *J Allergy Clin Immunol* 131(3):685–694.
15. Halapi E, et al. (2010) A sequence variant on 17q21 is associated with age at onset and severity of asthma. *Eur J Hum Genet* 18(8):902–908.
16. Leung TF, et al. (2009) Asthma and atopy are associated with chromosome 17q21 markers in Chinese children. *Allergy* 64(4):621–628.
17. Moffatt MF, et al. (2007) Genetic variants regulating ORMDL3 expression contribute to the risk of childhood asthma. *Nature* 448(7152):470–473.
18. Wu H, et al. (2009) Genetic variation in ORM1-like 3 (ORMDL3) and gasdermin-like (GSDML) and childhood asthma. *Allergy* 64(4):629–635.
19. Yu J, et al. (2011) Polymorphisms in GSDMA and GSDMB are associated with asthma susceptibility, atopy and BHR. *Pediatr Pulmonol* 46(7):701–708.
20. Tang MF, et al. (2016) Genetic effects of multiple asthma loci identified by genomewide association studies on asthma and spirometric indices. *Pediatr Allergy Immunol* 27(2):185–194.
21. Saleh NM, et al. (2011) Genetic association analyses of atopic illness and proinflammatory cytokine genes with type 1 diabetes. *Diabetes Metab Res Rev* 27(8):838–843.
22. Pal LR, Moult J (2015) Genetic basis of common human disease: Insight into the role of missense SNPs from genome-wide association studies. *J Mol Biol* 427(13):2271–2289.
23. Jostins L, et al.; International IBD Genetics Consortium (IIBDGC) (2012) Host-microbe interactions have shaped the genetic architecture of inflammatory bowel disease. *Nature* 491(7422):119–124.
24. Stahl EA, et al.; BIRAC Consortium; YEAR Consortium (2010) Genome-wide association study meta-analysis identifies seven new rheumatoid arthritis risk loci. *Nat Genet* 42(6):508–514.
25. Ding J, et al. (2016) Pore-forming activity and structural autoinhibition of the gasdermin family. *Nature* 535(7610):111–116.
26. Lin PH, Lin HY, Kuo CC, Yang LT (2015) N-terminal functional domain of Gasdermin A3 regulates mitochondrial homeostasis via mitochondrial targeting. *J Biomed Sci* 22(1):44.
27. Shi P, et al. (2015) Loss of conserved Gsdma3 self-regulation causes autophagy and cell death. *Biochem J* 468(2):325–336.
28. Kayagaki N, et al. (2015) Caspase-11 cleaves gasdermin D for non-canonical inflammasome signalling. *Nature* 526(7575):666–671.
29. Shi J, et al. (2015) Cleavage of GSDMD by inflammatory caspases determines pyroptotic cell death. *Nature* 526(7575):660–665.
30. Aglietti RA, et al. (2016) GsdmD p30 elicited by caspase-11 during pyroptosis forms pores in membranes. *Proc Natl Acad Sci USA* 113(28):7858–7863.
31. Chen X, et al. (2016) Pyroptosis is driven by non-selective gasdermin-D pore and its morphology is different from MLKL channel-mediated necroptosis. *Cell Res* 26(9):1007–1020.
32. Liu X, et al. (2016) Inflammasome-activated gasdermin D causes pyroptosis by forming membrane pores. *Nature* 535(7610):153–158.
33. Abecasis GR, et al.; 1000 Genomes Project Consortium (2012) An integrated map of genetic variation from 1,092 human genomes. *Nature* 491(7422):56–65.
34. Moon AF, Mueller GA, Zhong X, Pedersen LC (2010) A synergistic approach to protein crystallization: Combination of a fixed-arm carrier with surface entropy reduction. *Protein Sci* 19(5):901–913.
35. Krissinel E, Henrick K (2007) Inference of macromolecular assemblies from crystalline state. *J Mol Biol* 372(3):774–797.
36. Holm L, Sander C (1993) Protein structure comparison by alignment of distance matrices. *J Mol Biol* 233(1):123–138.
37. Saier MH, Jr, Tran CV, Barabote RD (2006) TCDB: The Transporter Classification Database for membrane transport protein analyses and information. *Nucleic Acids Res* 34(Database issue):D181–D186.
38. Van Dyk TK, Templeton LJ, Cantera KA, Sharpe PL, Sariaslani FS (2004) Characterization of the Escherichia coli AaeAB efflux pump: A metabolic relief valve? *J Bacteriol* 186(21):7196–7204.
39. Kumar S, van Raam BJ, Salvesen GS, Cieplak P (2014) Caspase cleavage sites in the human proteome: CaspDB, a database of predicted substrates. *PLoS One* 9(10):e110539.
40. Sampaio JL, et al. (2011) Membrane lipidome of an epithelial cell line. *Proc Natl Acad Sci USA* 108(5):1903–1907.
41. Takahashi T, Suzuki T (2012) Role of sulfatide in normal and pathological cells and tissues. *J Lipid Res* 53(8):1437–1450.
42. Wu W, et al. (2013) Regulation of integrin αV subunit expression by sulfatide in hepatocellular carcinoma cells. *J Lipid Res* 54(4):936–952.
43. Fuss IJ, et al. (2014) IL-13Rα2-bearing, type II NKT cells reactive to sulfatide self-antigen populate the mucosa of ulcerative colitis. *Gut* 63(11):1728–1736.
44. Das S, et al. (2016) GSDMB induces an asthma phenotype characterized by increased airway responsiveness and remodeling without lung inflammation. *Proc Natl Acad Sci USA* 113(46):13132–13137.
45. Grishina ZV, et al. (2008) Sulfatides inhibit leukotriene synthesis in human polymorphonuclear granulocytes by a mechanism involving lipid rearrangement in intracellular membranes. *Int J Biochem Cell Biol* 40(1):110–124.
46. Battye TG, Kontogiannis L, Johnson O, Powell HR, Leslie AG (2011) iMOSFLM: A new graphical interface for diffraction-image processing with MOSFLM. *Acta Crystallogr D Biol Crystallogr* 67(Pt 4):271–281.
47. McCoy AJ, et al. (2007) Phaser crystallographic software. *J Appl Cryst* 40(Pt 4):658–674.
48. Zhang KY, Cowtan K, Main P (1997) Combining constraints for electron-density modification. *Macromolecular Crystallography*, Methods in Enzymology, eds Carter CW, Sweet RM (Academic, New York), Vol 277, pp 53–64.
49. Murshudov GN, et al. (2011) REFMAC5 for the refinement of macromolecular crystal structures. *Acta Crystallogr D Biol Crystallogr* 67(Pt 4):355–367.
50. Emsley P, Lohkamp B, Scott WG, Cowtan K (2010) Features and development of Coot. *Acta Crystallogr D Biol Crystallogr* 66(Pt 4):486–501.
51. Robert X, Gouet P (2014) Deciphering key features in protein structures with the new ENDscript server. *Nucleic Acids Res* 42(Web Server issue):W320–W324.
52. Munnik T, Wierzchowiecka M (2013) Lipid-binding analysis using a fat blot assay. *Plant Lipid Signaling Protocols*, Methods in Molecular Biology, eds Munnik T, Heilmann I (Springer, New York), Vol 1009, pp 253–259.
53. Mui B, Chow L, Hope MJ (2003) Extrusion technique to generate liposomes of defined size. *Liposomes, Part A*, Methods in Enzymology, ed Duzgunes N (Academic, New York), Vol 367, pp 3–14.
54. Pop C, et al. (2001) Removal of the pro-domain does not affect the conformation of the procaspase-3 dimer. *Biochemistry* 40(47):14224–14235.
55. Notredame C, Higgins DG, Heringa J (2000) T-Coffee: A novel method for fast and accurate multiple sequence alignment. *J Mol Biol* 302(1):205–217.